

SOLAR DIFFERENTIAL ROTATION AND MERIDIONAL FLOW: THE ROLE OF A SUBADIABATIC TACHOCLINE FOR THE TAYLOR-PROUDMAN BALANCE

M. REMPEL

High Altitude Observatory, National Center for Atmospheric Research* , P.O. Box 3000, Boulder, Colorado 80307, USA
Draft version May 13, 2018

ABSTRACT

We present a simple model for the solar differential rotation and meridional circulation based on a mean field parameterization of the Reynolds stresses that drive the differential rotation. We include the subadiabatic part of the tachocline and show that this, in conjunction with turbulent heat conductivity within the convection zone and overshoot region, provides the key physics to break the Taylor-Proudman constraint, which dictates differential rotation with contour lines parallel to the axis of rotation in case of an isentropic stratification. We show that differential rotation with contour lines inclined by $10^\circ - 30^\circ$ with respect to the axis of rotation is a robust result of the model, which does not depend on the details of the Reynolds stress and the assumed viscosity, as long as the Reynolds stress transports angular momentum toward the equator. The meridional flow is more sensitive with respect to the details of the assumed Reynolds stress, but a flow cell, equatorward at the base of the convection zone and poleward in the upper half of the convection zone, is the preferred flow pattern.

Subject headings: Sun: interior — rotation — Sun: helioseismology

1. INTRODUCTION

Helioseismology has revealed detailed information about the internal rotation of the sun. Although the radiative interior of the Sun shows a roughly uniform rotation, the convection zone shows a differential rotation with a pole-equator difference of about 30% of the core rotation rate. The transition between the two regions is confined in a narrow shear layer, the so called tachocline, centered at about $0.7 R_\odot$ and having a thickness of about $0.04 R_\odot$ (Charbonneau et al. 1999). Within the convection zone the contours of constant angular velocity show in mid latitudes an inclination of about 25° with respect to the axis of rotation (Schou et al. 1998, 2002).

There is also robust observational evidence for a meridional flow, which is poleward near the surface and has a flow velocity around 20 m s^{-1} . This flow was first observed through movements of active regions and magnetic filaments (Labonte & Howard 1982; Topka et al. 1982) and later confirmed through helioseismology (see, e.g., Braun & Fan 1998; Haber et al. 2002; Zhao & Kosovichev 2004). Whereas most of the helioseismic studies focus only on the flow field very close to the surface (using local helioseismology), Braun & Fan (1998) used global helioseismology to extend their analysis further down and found a poleward meridional flow in the entire upper half of the convection zone. Even though the return flow has not been detected yet, it is self-evident that it is located in the lower half of the convection zone because of mass conservation. Since the density is significantly larger at the base of the convection zone, the flow amplitude can be very small there, on the order of a few m s^{-1} .

Following initial work by Glatzmaier & Gilman (1982) and Gilman & Miller (1986), differential rotation has been addressed over the past few decades by full spherical shell simulations of compressible convection.

Even though recent results by Miesch et al. (2000) and Brun & Toomre (2002) show improvement, the simulations still have problems in reproducing the radial gradient of the differential within the convection zone. Although the models predict the magnitude of the differential rotation (latitudinal variation) correctly, the contour lines of constant angular velocity are still very close to the Taylor-Proudman state with isolines parallel to the axis of rotation. The three-dimensional simulations also have problems in generating the observed meridional flow, which shows in the upper half of the convection zone a poleward flow of an amplitude of about 20 m s^{-1} . In contrast to observations, the three-dimensional simulations typically show several smaller flow cells of opposite sign and large temporal variability.

A completely different approach is based on axisymmetric mean field models that parametrize the turbulent angular momentum transport (Λ -effect; Kitchatinov & Rüdiger 1993). As discussed by Rüdiger et al. (1998), these models typically show solutions close to the Taylor-Proudman state unless a very large value of the turbulent viscosity is used.

Kitchatinov & Rüdiger (1995) showed that an anisotropic convective energy transport can produce a latitudinal variation in the temperature that is large enough to overcome the Taylor-Proudman constraint and allow for solar-like differential rotation while assuming reasonable values for the turbulent viscosity. The anisotropy of the energy flux results from the rotational influence on the turbulence modifying the turbulent heat diffusivities (Kitchatinov et al. 1994). Recently this model has been applied by Küker & Stix (2001) to study the evolution of the solar differential rotation of the Sun from the pre-main-sequence Sun to the present Sun by solving the momentum equations together with an mixing-length approach for the convective energy flux. The role of latitudinal variations of the entropy for the differential rotation was also studied by Durney (1999, 2003) within the framework of mean field models.

*The National Center for Atmospheric Research is sponsored by the National Science Foundation
Electronic address: rempel@hao.ucar.edu

In this paper we present a model that is along the lines of the axisymmetric mean field models mentioned above. Whereas the investigations of Kitchatinov & Rüdiger (1995) and Küker & Stix (2001) focused on the role of an anisotropic convective energy flux, we focus our investigation on the role of a subadiabatic tachocline for the Taylor-Proudman balance of the differential rotation. The aim of this paper is not to present a complete model for the solar differential rotation, but rather a simple approach to investigate the specific question of how a subadiabatic tachocline, in conjunction with turbulent heat conductivity within the convection zone and overshoot region, can break the Taylor-Proudman constraint which requires a differential rotation constant on cylinders in case of an isentropic stratification.

2. MODEL

In this investigation we use a simplified model for studying differential rotation and meridional circulation in the solar convection zone. The basic assumptions underlying this approach are as follows.

1. Axisymmetry and a spherically symmetric reference state.
2. All processes on the convective scale are parameterized, leading to turbulent viscosity, turbulent heat conductivity, and turbulent angular momentum transport.
3. The equations can be linearized assuming $\varrho_1 \ll \varrho_0$ and $p_1 \ll p_0$, and the reference state is assumed to be spherically symmetric. Here ϱ_0 and p_0 denote the reference state values, whereas ϱ_1 and p_1 are the perturbations caused by the presence of differential rotation. The equations we solve are the fully compressible, linearized, axisymmetric hydrodynamic equations.
4. The entropy equation includes only perturbations associated with differential rotation. Therefore, the reference state is assumed to be in an energy flux balance. It is further assumed that the effect of convection (in the convection zone and the overshoot region) on entropy perturbations associated with the differential rotation is purely diffusive.
5. The tachocline at the base of the solar convection zone is forced by a uniform rotation boundary condition at $r = 0.65 R_\odot$.

We emphasize that this model is not intended to be a complete solar convection zone model, since fundamental processes required for differential rotation such as turbulent angular momentum transport are parameterized.

This model is also intended to be a basis for a 'dynamic' flux-transport dynamo including the $\mathbf{j} \times \mathbf{B}$ force feedback on meridional flow and differential rotation (future work).

2.1. Basic equations

For this model we use the axisymmetric, fully compressible hydrodynamic equations. Since the perturbation of pressure and density caused by the differential rotation are small compared with the reference state values [$\varrho_1/\varrho_0 \sim p_1/p_0 \sim (\Delta\Omega R_\odot/c_s)^2 \sim 10^{-5}$], we linearize

the equations, assuming $\varrho_1 \ll \varrho_0$ and $p_1 \ll p_0$. Since we do not use the anelastic approximation here (see section 2.6 for more details), we keep the time derivative in the continuity equation:

$$\frac{\partial \varrho_1}{\partial t} = -\frac{1}{r^2} \frac{\partial}{\partial r} (r^2 v_r \varrho_0) - \frac{1}{r \sin \theta} \frac{\partial}{\partial \theta} (\sin \theta v_\theta \varrho_0), \quad (1)$$

$$\begin{aligned} \frac{\partial v_r}{\partial t} = & -v_r \frac{\partial v_r}{\partial r} - \frac{v_\theta}{r} \frac{\partial v_r}{\partial \theta} + \frac{v_\theta^2}{r} - \frac{1}{\varrho_0} \left(\varrho_1 g(r) + \frac{\partial p_1}{\partial r} \right) \\ & + (2\Omega_0 \Omega_1 + \Omega_1^2) r \sin^2 \theta + \frac{F_r}{\varrho_0}, \end{aligned} \quad (2)$$

$$\begin{aligned} \frac{\partial v_\theta}{\partial t} = & -v_r \frac{\partial v_\theta}{\partial r} - \frac{v_\theta}{r} \frac{\partial v_\theta}{\partial \theta} - \frac{v_r v_\theta}{r} - \frac{1}{\varrho_0} \frac{1}{r} \frac{\partial p_1}{\partial \theta} \\ & + (2\Omega_0 \Omega_1 + \Omega_1^2) r \sin \theta \cos \theta + \frac{F_\theta}{\varrho_0}, \end{aligned} \quad (3)$$

$$\begin{aligned} \frac{\partial \Omega_1}{\partial t} = & -\frac{v_r}{r^2} \frac{\partial}{\partial r} [r^2 (\Omega_0 + \Omega_1)] \\ & - \frac{v_\theta}{r \sin^2 \theta} \frac{\partial}{\partial \theta} [\sin^2 \theta (\Omega_0 + \Omega_1)] + \frac{F_\phi}{\varrho_0 r \sin \theta}, \end{aligned} \quad (4)$$

$$\begin{aligned} \frac{\partial s_1}{\partial t} = & -v_r \frac{\partial s_1}{\partial r} - \frac{v_\theta}{r} \frac{\partial s_1}{\partial \theta} + v_r \frac{\gamma \delta}{H_p} + \frac{\gamma - 1}{p_0} Q \\ & + \frac{1}{\varrho_0 T_0} \operatorname{div}(\kappa_t \varrho_0 T_0 \operatorname{grad} s_1), \end{aligned} \quad (5)$$

where

$$p_1 = p_0 \left(\gamma \frac{\varrho_1}{\varrho_0} + s_1 \right), \quad (6)$$

$$H_p = \frac{p_0}{\varrho_0 g}. \quad (7)$$

We use here the dimensionless entropy $s = \ln(p/\varrho^\gamma)$, meaning that the entropy equation Eq. (5) was made dimensionless by division through $c_v = (\gamma - 1)^{-1} R/\mu$.

The third term on the right-hand side of Eq. (5) describes the effects of a non-adiabatic reference state, where $\delta = \nabla - \nabla_{\text{ad}}$ is related to the gradient of the reference state entropy through:

$$\frac{ds_0}{dr} = -\frac{\gamma \delta}{H_p}. \quad (8)$$

The fourth term in Eq. (5) considers the energy transfer through Reynolds stress that will be defined in detail in the following paragraph. The last term describes turbulent diffusion of entropy perturbation within the convection zone, where κ_t denotes the turbulent thermal diffusivity. We neglect in Eq. (5) the contribution of the radiative energy flux, since even for overshoot values the turbulent heat conductivity exceeds the radiative one by several orders of magnitude.

The viscous force \mathbf{F} follows from

$$\begin{aligned} F_r = & \frac{1}{r^2} \frac{\partial}{\partial r} (r^2 R_{rr}) + \frac{1}{r \sin \theta} \frac{\partial}{\partial \theta} (\sin \theta R_{\theta r}) \\ & - \frac{R_{\theta\theta} + R_{\phi\phi}}{r}, \end{aligned} \quad (9)$$

$$\begin{aligned} F_\theta = & \frac{1}{r^2} \frac{\partial}{\partial r} (r^2 R_{r\theta}) + \frac{1}{r \sin \theta} \frac{\partial}{\partial \theta} (\sin \theta R_{\theta\theta}) \\ & + \frac{R_{r\theta} - R_{\phi\phi} \cot \theta}{r}, \end{aligned} \quad (10)$$

$$\begin{aligned} F_\phi = & \frac{1}{r^2} \frac{\partial}{\partial r} (r^2 R_{r\phi}) + \frac{1}{r \sin \theta} \frac{\partial}{\partial \theta} (\sin \theta R_{\theta\phi}) \\ & + \frac{R_{r\phi} + R_{\theta\phi} \cot \theta}{r}, \end{aligned} \quad (11)$$

with the Reynolds stress tensor

$$R_{ik} = -\varrho_0 \langle v'_i v'_k \rangle = \nu_t \varrho_0 \left(E_{ik} - \frac{2}{3} \delta_{ik} \operatorname{div} \mathbf{v} + \Lambda_{ik} \right). \quad (12)$$

Here $E_{ik} = v_{i;k} + v_{k;i}$ denotes the deformation tensor, which is given in spherical coordinates by

$$E_{rr} = 2 \frac{\partial v_r}{\partial r}, \quad (13)$$

$$E_{\theta\theta} = 2 \frac{1}{r} \frac{\partial v_\theta}{\partial \theta} + 2 \frac{v_r}{r}, \quad (14)$$

$$E_{\phi\phi} = \frac{2}{r} (v_r + v_\theta \cot \theta), \quad (15)$$

$$E_{r\theta} = E_{\theta r} = r \frac{\partial}{\partial r} \frac{v_\theta}{r} + \frac{1}{r} \frac{\partial v_r}{\partial \theta}, \quad (16)$$

$$E_{r\phi} = E_{\phi r} = r \sin \theta \frac{\partial \Omega_1}{\partial r}, \quad (17)$$

$$E_{\theta\phi} = E_{\phi\theta} = \sin \theta \frac{\partial \Omega_1}{\partial \theta}, \quad (18)$$

whereas Λ_{ik} denotes the non diffusive Reynolds stresses, which are responsible for driving differential rotation. We will discuss these terms later.

The amount of energy that is converted by the Reynolds stress is given by:

$$Q = \sum_{i,k} \frac{1}{2} E_{ik} R_{ik}. \quad (19)$$

Q contains a heating term resulting from the dissipation of kinetic energy through the dissipative contribution to the Reynolds stress (terms proportional to E_{ik}) and a cooling term resulting from the energy transfer introduced by the nondiffusive transport term proportional to Λ_{ik} responsible for maintaining the differential rotation. The latter is in general the dominant term. The importance of the term Q for a stationary solution becomes more apparent if we transform the entropy equation to an equation of the quantity $\varrho_0 T_0 s_1$, which better represents the energy perturbation associated with the entropy perturbation. In the case of a stationary solution, we have $\operatorname{div}(\varrho_0 \mathbf{v}) = 0$ and we can rewrite the entropy equation Eq. (5) in the form (assuming $|\delta| = |\nabla - \nabla_{\text{ad}}| \ll 1$)

$$\operatorname{div}(\mathbf{v} \varrho_0 T_0 s_1 - \kappa_t \varrho_0 T_0 \operatorname{grad} s_1) = (\gamma - 1) \left[\frac{\varrho_0 T_0}{p_0} Q - v_r \frac{\varrho_0 T_0 s_1}{\gamma H_p} \right] + v_r \gamma \delta \frac{\varrho_0 T_0}{H_p}. \quad (20)$$

The terms that appear in this equation are the divergence of the energy flux (left-hand side), a source term that considers the viscous heating and the buoyancy work (first term, right-hand side), and the source term that arises from the nonadiabatic stratification (second term, right-hand side). The first term redistributes $\varrho_0 T_0 s_1$ but does not provide a net source, since the flux across the boundaries vanishes with the boundary conditions we use. The same applies to the last term in the case of a stationary solution, since the horizontal mean of the radial mass flux $v_r \varrho_0$ has to vanish and δ and g show no latitudinal dependence. The only net source is the second term, which contains the Reynolds stress and buoyancy work. In the case of a stationary solution the volume integral of this term has to vanish, which means that the energy extracted through the Λ -effect from the reservoir

of internal energy (through feedback on convective motions) returns through viscous heating and work of the meridional flow against the buoyant force.

2.2. Background stratification

For the background ϱ_0 , p_0 , and T_0 we use an adiabatic hydrostatic stratification assuming an $\sim r^{-2}$ dependence of the gravitational acceleration given by

$$T_0(r) = T_{\text{bc}} \left[1 + \frac{\gamma - 1}{\gamma} \frac{r_{\text{bc}}}{H_{\text{bc}}} \left(\frac{r_{\text{bc}}}{r} - 1 \right) \right], \quad (21)$$

$$p_0(r) = p_{\text{bc}} \left[1 + \frac{\gamma - 1}{\gamma} \frac{r_{\text{bc}}}{H_{\text{bc}}} \left(\frac{r_{\text{bc}}}{r} - 1 \right) \right]^{\gamma/(\gamma-1)}, \quad (22)$$

$$\varrho_0(r) = \varrho_{\text{bc}} \left[1 + \frac{\gamma - 1}{\gamma} \frac{r_{\text{bc}}}{H_{\text{bc}}} \left(\frac{r_{\text{bc}}}{r} - 1 \right) \right]^{1/(\gamma-1)}, \quad (23)$$

$$g(r) = g_{\text{bc}} \left(\frac{r}{r_{\text{bc}}} \right)^{-2}, \quad (24)$$

where T_{bc} , p_{bc} , and ϱ_{bc} denote the values of temperature, pressure and density at the base of the convection zone $r = r_{\text{bc}}$. Here $H_{\text{bc}} = p_{\text{bc}}/(\varrho_{\text{bc}} g_{\text{bc}})$ is the pressure scale height and g_{bc} the value of the gravity at r_{bc} . In the following we use $r_{\text{bc}} = 0.71 R_\odot$, $p_{\text{bc}} = 6 \times 10^{12}$ Pa, $\varrho_{\text{bc}} = 200 \text{ kg m}^{-3}$, $g_{\text{bc}} = 520 \text{ m s}^{-2}$, and $R_\odot = 7 \times 10^8 \text{ m}$, which results in $H_{\text{bc}} = 0.0825 R_\odot$.

2.3. Superadiabaticity profile

For the superadiabaticity δ we assume the following profile:

$$\delta = \delta_{\text{conv}} + \frac{1}{2} (\delta_{\text{os}} - \delta_{\text{conv}}) \left(1 - \tanh \left(\frac{r - r_{\text{tran}}}{d_{\text{tran}}} \right) \right), \quad (25)$$

where

$$\delta_{\text{conv}} = \delta_{\text{top}} \exp\left(\frac{r - r_{\text{max}}}{d_{\text{top}}}\right) + \delta_{\text{cz}} \frac{r - r_{\text{sub}}}{r_{\text{max}} - r_{\text{sub}}}. \quad (26)$$

Here δ_{top} , δ_{cz} , and δ_{os} denote the values of superadiabaticity at the top of the domain $r = r_{\text{max}}$, in the bulk of the convection zone, and in the overshoot region, respectively. In addition r_{sub} denotes the radius at which the stratification within the convection zone turns weakly subadiabatic (because of nonlocal effects), and r_{tran} denotes the radius of transition towards stronger subadiabatic stratification (the overshoot region). The parameters d_{top} and d_{tran} determine the steepness of the transition toward large superadiabaticities at the top of the domain and towards the overshoot region, respectively. Fig. 1 shows the profiles of the superadiabaticity we use later in our models.

Nonlocal mixing-length models show a transition from subadiabatic to superadiabatic values typically between $r = 0.75$ and $0.8 R_\odot$ depending on the assumed mixing-length parameter (Pidatella & Stix 1986; Skaley & Stix 1991). For larger degrees of non-locality the subadiabatic fraction of the convection zone could be even larger (Spruit 1997; Rempel 2004). Mixing-length models predict a variation of δ within the convection zone by several orders of magnitude; however, most of this variation occurs very close to the surface layers, which are difficult to resolve in a mean field model. Since our model captures only the large-scale flows, we also have to make

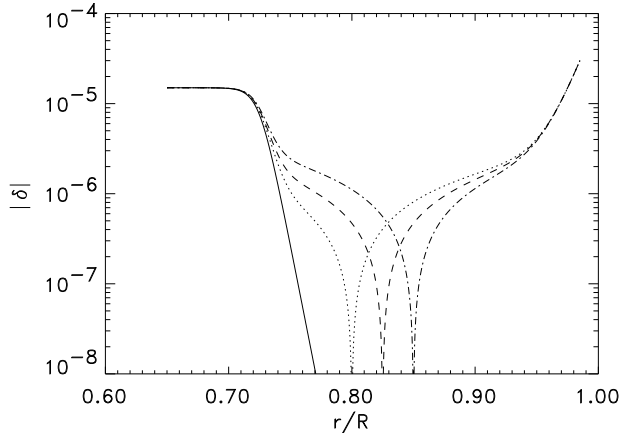


FIG. 1.— Profile of superadiabaticity used in the models with adiabatic convection zone (solid line), model 8 (dotted line), model 9 (dashed line), and model 10 (dashed-dotted line). In all cases we have $\delta_{\text{os}} = -1.5 \times 10^{-5}$, $r_{\text{tran}} = 0.725 R_{\odot}$, and $d_{\text{tran}} = 0.0125 R_{\odot}$. Common parameters of the models 8 to 10 are $d_{\text{top}} = 0.0125 R_{\odot}$, $\delta_{\text{cz}} = 3 \times 10^{-6}$, and $\delta_{\text{top}} = 3 \times 10^{-5}$. Case 8 shows a profile with $r_{\text{sub}} = 0.8 R_{\odot}$, case 9 with $r_{\text{sub}} = 0.825 R_{\odot}$, and case 10 with $r_{\text{sub}} = 0.85 R_{\odot}$. Shown on the vertical axis is $|\delta|$ on a logarithmic scale. The singularities at $r = 0.8, 0.825, \text{ and } 0.85 R_{\odot}$ indicate where δ changes sign in the models with a nonadiabatic convection zone.

sure that the Rayleigh number stays sub critical for convection within the domain for the thermal conductivity and viscosity we use.

In this investigation we keep the following parameters fixed: $d_{\text{top}} = d_{\text{tran}} = 0.0125 R_{\odot}$ and $r_{\text{tran}} = 0.725 R_{\odot}$. Choosing a value of $\delta_{\text{top}} = 3 \times 10^{-5}$ we have to use a thermal diffusivity of around $5 \times 10^9 \text{ m}^2 \text{ s}^{-1}$. Much larger values of δ would require unreasonably large values of the turbulent heat conductivity. Below $r = r_{\text{tran}}$ we assume overshoot type values of the superadiabaticity, in the range -10^{-5} to -10^{-4} . We extend our domain down to $r = 0.65 R_{\odot}$, which also includes the radiative interior with values of $\delta \sim -0.1$. Since our diffusivity profile (see next subsection) drops significantly below r_{bc} , the entropy perturbation generated at the lower boundary does not influence the values within the convection zone and has therefore no influence on the differential rotation profile. More important for this model is the overlap between the subadiabatic region and the thermal diffusivity profile, since this determines to what extent an entropy perturbation can spread from the subadiabatic region into the convection zone. Since the representation of a strongly subadiabatic layer would cause numerical difficulties (see section 2.6 for further details) we decided to exclude this layer and use overshoot values for δ down to $0.65 R_{\odot}$. The effective thickness of the overshoot is determined by the overlap with the thermal conductivity profile, which we define in the next subsection. Since the heat conductivity is basically zero below $r_{\text{bc}} = 0.71 R_{\odot}$, the effective thickness of the overshoot region is about $2 d_{\text{tran}} \approx 20 \text{ Mm}$, which is in the range of predictions of nonlocal mixing-length models (Pidatella & Stix 1986; Skaley & Stix 1991).

Since all these values are small compared with ∇_{ad} , we still can use the adiabatic reference state for pressure,

density, and temperature as given above in Eqs. (21) and (23).

2.4. Diffusivity profiles

For the turbulent viscosity and thermal conductivity we assume constant values within the convection zone and the radiative zone with a transition smoothed by a hyperbolic tangent function. We assume that the diffusivities only depend on the radial coordinate:

$$\nu_t = \frac{\nu_0}{2} \left[1 + \tanh \left(\frac{r - r_{\text{tran}} + \Delta}{d_{\kappa\nu}} \right) \right] f_c(r), \quad (27)$$

$$\kappa_t = \frac{\kappa_0}{2} \left[1 + \tanh \left(\frac{r - r_{\text{tran}} + \Delta}{d_{\kappa\nu}} \right) \right] f_c(r), \quad (28)$$

with

$$f_c(r) = \frac{1}{2} \left[1 + \tanh \left(\frac{r - r_{\text{bc}}}{d_{\text{bc}}} \right) \right], \quad (29)$$

$$\Delta = d_{\kappa\nu} \tanh^{-1} (2\alpha_{\kappa\nu} - 1), \quad (30)$$

where ν_0 and κ_0 denote the values of the turbulent diffusivities within the convection zone and $\alpha_{\kappa\nu}$ specifies the values of the turbulent diffusivities at $r = r_{\text{tran}}$ ($\alpha_{\kappa\nu}\nu_0$, $\alpha_{\kappa\nu}\kappa_0$), where the transition to the overshoot region takes place in our model. The profile function f_c ensures that the diffusivities drop significantly toward the radiative interior at r_{bc} . For the width of this transition we use $d_{\text{bc}} = 0.0125 R_{\odot}$. Since both diffusivities are of turbulent origin, we use the same radial profile.

In this model we do not include a sophisticated theory for the tachocline but force a tachocline through a uniform rotation boundary at $r = 0.65 R_{\odot}$. As a consequence the tachocline is a viscous shear layer between the convection zone and the lower boundary condition. We therefore have to maintain a sufficient amount of viscosity in the radiative interior to allow for the formation of this shear layer in a reasonable amount of time. In the following we use the profile defined by Eq. (27) for the computation of the turbulent angular momentum transport (last term in Eq. [12]) but set the viscosity used for the diffusive terms of the Reynolds stress (first two terms in Eq. [12]) to 2% of the convection zone values. For the heat conductivity we use in the radiative interior 0.2% of the convection zone values.

2.5. Parameterization of turbulent angular momentum transport

The terms relevant for the differential rotation are:

$$\Lambda_{r\phi} = \Lambda_{\phi r} = +L(r, \theta) \cos(\theta + \lambda(r, \theta)), \quad (31)$$

$$\Lambda_{\theta\phi} = \Lambda_{\phi\theta} = -L(r, \theta) \sin(\theta + \lambda(r, \theta)), \quad (32)$$

where $L(r, \theta)$ denotes the amplitude of the angular momentum flux, whereas $\lambda(r, \theta)$ describes the inclination of the flux vector with respect to the axis of rotation.

Symmetry considerations require that $\Lambda_{r\phi}$ is symmetric and $\Lambda_{\theta\phi}$ is antisymmetric across the equator. To satisfy this constraint, $\lambda(r, \theta)$ and $L(r, \theta)$ need to be antisymmetric functions with respect to the equator. Since we solve our model only in the northern hemisphere, we specify in the following discussion always values for λ and L in the northern hemisphere. To maintain the proper symmetry for a full-sphere simulation, values for

the southern hemisphere would have to be chosen by reflection across the equator.

The setting $L > 0$, $\lambda = 0$ corresponds to a flux directed downward and parallel to the axis of rotation; $L > 0$, $\lambda = -\theta$ to a radially inward flux, and $L > 0$, $\lambda = \pi/2 - \theta$ to an equatorward flux. The setting $L \sim \sin \theta \cos \theta$ and $\lambda = 0$ recovers the limit of fast rotation found for the Λ -effect by Kitchatinov & Rüdiger (1995).

In the following discussion we will for the amplitude of the angular momentum flux the expression

$$f(r, \theta) = (\sin \theta)^n \cos \theta \tanh \left(\frac{r_{\max} - r}{d} \right),$$

$$L(r, \theta) = \Lambda_0 \Omega_0 \frac{f(r, \theta)}{\max |f(r, \theta)|}. \quad (33)$$

The full radial dependence of the angular momentum flux is obtained by multiplication by $\nu_t \varrho_0$. The angular momentum flux drops below r_{tran} because of the drop in turbulent viscosity. In most of the following discussion we require a vanishing angular momentum flux at the top boundary as expressed in Eq. (33), where we use a value of $d = 0.025 R_\odot$ for the transition layer at the top. The exponent n determines the latitude at which the flux peaks. For $\lambda > 0$, the value of n needs to be larger than 2 to ensure the regularity of the divergence of the Reynolds stress close to the pole. For the direction of the flux determined by λ we discuss two distinct cases: $\lambda = 15^\circ$ (transport nearly parallel to axis of rotation) and $\lambda = 90^\circ - \theta$ (transport in latitude only) in order to evaluate the sensitivity of the model with respect to this parameterization.

2.6. Numerical procedure

We are interested here in the stationary solution of Eqs. (1) to (5) for a given parameterization of the turbulent angular momentum transport Eq. (31), (32). A very natural way to relax the system is to use the temporal evolution; however, because of the low Mach number of the expected flows, a direct compressible simulation is problematic. For an expected meridional flow velocity of a few m s^{-1} the Mach number is around 10^{-5} (because of axisymmetry, the much faster differential rotation flow does not enter the time step limit). Without leaving the regime of highly subsonic flows and therefore without changing the physical properties of the solution, it is possible to speed up the relaxation process significantly by increasing the base rotation rate Ω_0 .

Using the following transformation for the independent parameters of the equations,

$$\begin{aligned} \Omega_0 &\longrightarrow \zeta \Omega_0, \\ \nu_t &\longrightarrow \zeta \nu_t, \\ \kappa_t &\longrightarrow \zeta \zeta \kappa_t, \\ \delta &\longrightarrow \zeta^2 \delta, \\ t &\longrightarrow \zeta^{-1} t, \end{aligned}$$

and the following transformation for variables,

$$\begin{aligned} v_r &\longrightarrow \zeta v_r, \quad v_\theta \longrightarrow \zeta v_\theta, \quad \Omega_1 \longrightarrow \zeta \Omega_1, \\ p_1 &\longrightarrow \zeta^2 p_1, \quad \varrho_1 \longrightarrow \zeta^2 \varrho_1, \quad s_1 \longrightarrow \zeta^2 s_1, \end{aligned} \quad (34)$$

Eqs. (2) - (5) remain unchanged, meaning that if $\{\varrho_1, v_r, v_\theta, \Omega_1, s_1\}$ is a solution for the parameters

$\{\Omega_0, \nu_t, \kappa_t, \delta\}$ then $\{\zeta^2 \varrho_1, \zeta v_r, \zeta v_\theta, \zeta \Omega_1, \zeta^2 s_1\}$ is a solution for the parameters $\{\zeta \Omega_0, \zeta \nu_t, \zeta \kappa_t, \zeta^2 \delta\}$. However this transformation changes the equation of continuity to:

$$\frac{\partial \varrho_1}{\partial t} + \frac{1}{\zeta^2} \text{div}(\varrho_0 \mathbf{v}) = 0, \quad (35)$$

meaning that the time evolution is changed, but the stationary solution remains unchanged. The pre factor ζ^{-2} in the equation of continuity corresponds to the increase of the Mach number of the flow by a factor of ζ . In the following we use a value of $\zeta = 100$, which corresponds to an increase of the Mach number of the meridional flow in the bulk of the convection zone from 10^{-5} to 10^{-3} . Therefore even the time evolution is only marginally affected, since the solution stays in the regime of highly subsonic flows. We computed solutions with different values of ζ in order to quantify the influence of this transformation. We found differences between a solution computed with $\zeta = 10$ and 100 on the order of a few percent (mainly in the magnitude of the differential rotation close to the pole).

This approach is very similar to simulations of rising magnetic flux tubes in the solar convection zone, which were made fully compressible by assuming a value of $\beta = p_{\text{gas}}/p_{\text{mag}}$ on the order of 100 instead of 10^5 to overcome a severe time step constraint. As long as the relevant flow velocities remain sufficiently subsonic, the results are not affected significantly.

The only drawback of this approach is that it is impossible to represent large values of the subadiabaticity as found in the radiative interior of the Sun. Because of the scaling of δ with ζ^2 , a value of $\delta = -0.1$ would correspond to $\delta = -1000$ in a solution with a base rotation increased by a factor of 100, which is physically impossible. However, overshoot-like values of $\delta \sim -10^{-5}$ can be treated without any problem. As we explained earlier in subsection 2.3 and 2.4, the radiative interior is not of great importance, since entropy perturbations created there cannot influence the convection zone we are primarily interested in.

Since our model also includes a significant time step constraint because of the large turbulent diffusivities in the convection zone, an anelastic approach would not provide much advantage unless all diffusivities were treated implicitly. We therefore decided to solve the equations with a faster explicit scheme using the procedure outlined above. We tested an anelastic version of the code and found convergence problems of the pressure solver related to the uniform rotation boundary that we impose at $r = 0.65 R_\odot$. For a different choice of boundary conditions we found very good agreement between the anelastic version and a solution computed with $\zeta = 100$ as described above.

We solve Eqs. (1) - (5) with a MacCormack scheme using alternating upwind and downwind differencing, which is second order in space and time. The computational domain extends in latitude from equator to pole and in radius from $r = 0.65$ to $0.985 R_\odot$. We use the appropriate symmetry boundary conditions at equator and pole and closed boundaries in radius. At the bottom boundary ($r = 0.65 R_\odot$) we enforce a uniform rotation; the top boundary is stress-free for the angular velocity ($R_{r\phi} = 0$). At both radial boundaries we use stress-free boundary

TABLE 1
SIGNIFICANT PARAMETERS OF SIMPLIFIED MODEL

| case | λ | n | $d_{\kappa\nu}$ | $\alpha_{\kappa\nu}$ | δ_{os} | r_{sub} |
|------|---------------------|-----|-----------------|----------------------|-----------------------|------------------|
| 1 | 15° | 2 | 0.025 | 0.1 | -1.5×10^{-5} | |
| 2 | $90^\circ - \theta$ | 2 | 0.025 | 0.1 | -1.5×10^{-5} | |
| 3 | 15° | 2 | 0.025 | 0.1 | 0 | |
| 4 | 15° | 4 | 0.025 | 0.1 | -1.5×10^{-5} | |
| 5 | 15° | 2 | 0.025 | 0.1 | -3×10^{-5} | |
| 6 | 15° | 2 | 0.05 | 0.1 | -1.5×10^{-5} | |
| 7 | 15° | 2 | 0.025 | 0.025 | -1.5×10^{-5} | |
| 8 | 15° | 2 | 0.025 | 0.1 | -1.5×10^{-5} | 0.8 |
| 9 | 15° | 2 | 0.025 | 0.1 | -1.5×10^{-5} | 0.825 |
| 10 | 15° | 2 | 0.025 | 0.1 | -1.5×10^{-5} | 0.85 |

NOTE. — Cases 1 - 7 have adiabatic convection zones and cases 8 - 10 have nonadiabatic convection zones with, the common parameters $\delta_{\text{cz}} = 3 \times 10^{-6}$ and $\delta_{\text{top}} = 3 \times 10^{-5}$, but different values of r_{sub} , as shown in the table.

conditions for the velocity and set the derivative of s_1 to zero. Since we focus in this study on the large-scale flow fields, a moderate resolution of around 108 grid points in radius and 72 grid points in latitude is sufficient. We tested our code by reproducing the result presented by Rüdiger et al. (1998, their Fig. 1).

3. RESULTS

Since our simplified model contains parameterizations of crucial processes, we have to evaluate carefully the dependence on particular choices of these parameters. In Table 1 we have summarized the parameters that we discuss in this section. There are additional model parameters, which do not have a significant influence on the solution. These are r_{tran} , Λ_0 , ν_0 , and κ_0 . Here r_{tran} specifies where the superadiabaticity turns from convection zone to overshoot values. In the following we use $r_{\text{tran}} = 0.725 R_\odot$, which is a reasonable choice for the Sun. As long as $r_{\text{tran}} > r_{\text{bc}} + d_{\text{bc}}$ the influence on the solution is small, since it is more the profile of ν_t and κ_t in relation to r_{tran} that matters. We have therefore introduced in Eqs. (27) and (28) the parameter $\alpha_{\kappa\nu}$, which specifies the profile relative to r_{tran} . Similarly Λ_0 specifies the magnitude of the nondiffusive Reynolds-stress (Λ -effect). Typical values for Λ_0 are on the order of unity. Except for case 2, in which we use $\Lambda_0 = 0.4$, in the following we use a value of $\Lambda_0 = 0.8$. We have chosen Λ_0 such that the magnitude of the differential rotation is close to solar-like.

For the diffusivities ν_0 and κ_0 we assume in the following discussion $\nu_0 = \kappa_0 = 5 \times 10^8 \text{ m}^2 \text{ s}^{-1}$. For cases with a superadiabatic convection zone we have to increase the value of κ_0 to $5 \times 10^9 \text{ m}^2 \text{ s}^{-1}$ above r_{sub} in order to avoid convective instability.

3.1. General solution properties: differential rotation

The key ingredient in this model is the inclusion of a subadiabatic tachocline beneath the convection zone, which is enforced in this model through the uniform rotation lower boundary condition. Within the subadiabatic region ($r \lesssim 0.725 R_\odot$) the differential rotation is balanced by a latitudinal entropy gradient. Taking the curl of the meridional momentum equation yields for the

ϕ component of the vorticity under the assumption of small deviations from adiabaticity ($|\nabla - \nabla_{\text{ad}}| \ll 1$)

$$\frac{\partial \omega_\phi}{\partial t} = [\dots] + r \sin \theta \frac{\partial \Omega^2}{\partial z} - \frac{g}{\gamma r} \frac{\partial s_1}{\partial \theta} \quad (36)$$

with $\Omega = \Omega_0 + \Omega_1$; the bracket denotes viscous terms and vorticity transport terms, which are not important for the following discussion.

Starting initially with $s_1 = 0$, the turbulent angular momentum transport leads to a negative values of $\partial \Omega^2 / \partial z$ in high latitudes, which enforces a negative value of ω_ϕ . A negative value of ω_ϕ corresponds to a counter-clockwise meridional flow in the tachocline, which shows a negative radial velocity at high latitudes and a positive velocity at low latitudes. Because of the subadiabatic stratification, this results in a positive entropy perturbation in high latitudes and a negative entropy perturbation in low latitudes, as shown in Fig. 2 b). Since the resulting negative value of $\partial s_1 / \partial \theta$ can compensate for the also negative value of $\partial \Omega^2 / \partial z$, an equilibrium is reached finally. An additional source for the entropy perturbations comes from the meridional flow driven in the convection zone and penetrating to some extent into the subadiabatic overshoot region. For the parameters used in this model both effects are of roughly the same order of magnitude. In our model most of the tachocline shear is located below the base of the convection zone, whereas helioseismic inversions find more overlap between the tachocline and the convection zone (Charbonneau et al. 1999). Our model has therefore most probably the tendency to underestimate the entropy perturbation in the overshoot region caused by the value of $\partial \Omega^2 / \partial z$.

Because of the turbulent thermal heat conductivity this entropy perturbation can spread into the convection zone and therefore also balance there a differential rotation that deviates from the Taylor-Proudman state with Ω -contours parallel to the axis of rotation. We want to emphasize that the total entropy $s_0 + s_1$ in the overshoot region is still smaller than in the convection zone. The physical reason for this spread is that the convection tries to maintain the same radial entropy gradient at all latitudes (if we do not consider possible rotational anisotropy). Since the overshoot region provides the entropy boundary condition for the convection zone, a latitudinal variation of entropy in the overshoot region is transported by convection into the convection zone. Stix (1981) computed response functions for the temperature, velocity, and flux perturbations within in the framework of the mixing-length approach and found that the screening effect of temperature perturbations is very weak, meaning that temperature (entropy) perturbations at the base of the convection zone should be transmitted through the entire convection zone.

The magnitude of the entropy perturbation in the convection zone depends on the overlap between the thermal conductivity profile and the subadiabaticity profile. For most models we use a parameter of $\alpha_{\kappa\nu} = 0.1$, which means that the thermal diffusivity drops to 10% of its convection zone values at $r = r_{\text{tran}} = 0.725 R_\odot$, but smaller values ($\alpha_{\kappa\nu} = 0.025$) also work if the value of δ_{os} is slightly increased (see cases 5 and 7). The thermal heat diffusivity in a nonlocal mixing-length model, $\sim v_{\text{conv}} H_p$, would lead to larger values within the overshoot region because of the large value of the pressure

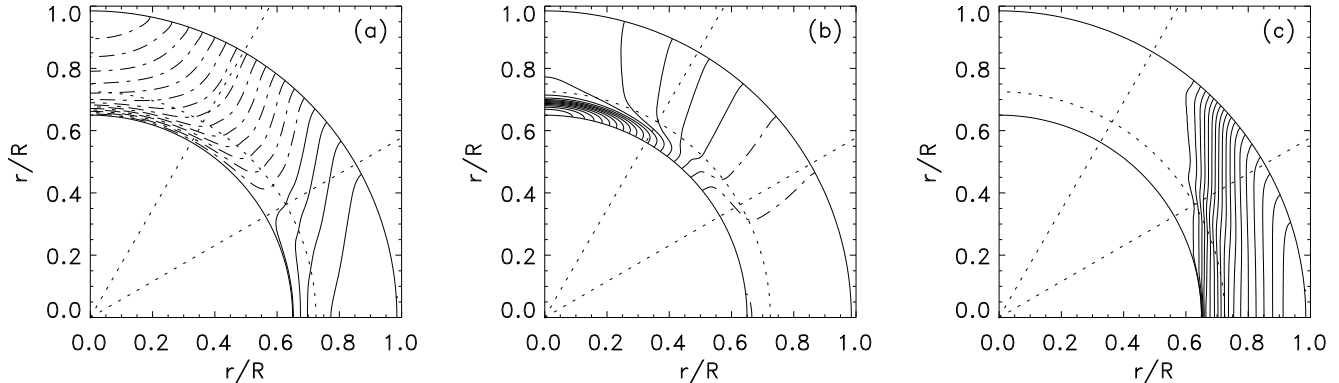


FIG. 2.— Contours of (a) differential rotation and (b) entropy perturbation for case 1. Solid lines indicate positive values. The entropy perturbation that originates in the subadiabatic tachocline and spreads because of thermal conductivity into the convection zone prevents the Taylor-Proudman state (contours parallel to axis of rotation) for the differential rotation from developing. (c) Contours of differential rotation for case 3. This case is similar to case 1, except that $s_1 = 0$. As a consequence the contour lines of constant Ω are aligned with the axis of rotation.

scale height and still significant velocities $\sim 10 \text{ ms}^{-1}$ in the overshoot region.

The temperature perturbation associated with the entropy perturbation shows a magnitude of about 5K throughout the convection zone for most of our models. Whereas the entropy perturbation drops monotonically from pole to equator, the temperature perturbation close to the surface reaches a minimum around mid latitudes followed by a slight increase toward the equator. At the base of the convection zone the temperature also shows a monotonic decrease from the pole toward the equator. The different behavior of entropy and temperature is due to the pressure perturbation within the convection zone, which also contains an adiabatic contribution (first term on right-hand side of Eq. [6]). A similar pattern was also found by Brun & Toomre (2002) in three-dimensional simulations; however, the physical reason might be different.

In Fig. 2 we show the contours of Ω and the related entropy perturbation s_1 for case 1. Since the entropy perturbation is concentrated in higher latitudes (where $\partial\Omega^2/\partial z$ also peaks), the deviations from the Taylor-Proudman state are largest in high latitudes. Whereas the differential rotation shows close to the pole Ω -contours perpendicular to the axis of rotation, the Ω -contours are more aligned with the axis of rotation close to the equator.

In Fig. 2 c) we show for reference purposes a solution with $s_1 = 0$ but, apart from that, exactly the same parameters as case 1. Without the effect of the subadiabatic tachocline the solution shows differential rotation with cylindrical Ω contours, even though we still impose the uniform rotation boundary condition at $r = 0.65 R_\odot$.

3.2. General solution properties: meridional flow

Since the assumed turbulent angular momentum transport has in general the tendency to drive a differential rotation that differs from the profile that would balance the right-hand side of Eq. (36), the differential rotation shows a small perturbation around this state. As a consequence, the Coriolis force related to this perturbation cannot be precisely balanced by a combination of pres-

sure gradient and buoyancy and therefore drives a meridional flow (examples of this flow can be seen in Fig. 4). This flow grows until the additional angular momentum transport sufficiently limits the perturbation of Ω so that the remaining weak unbalanced Coriolis force can be balanced by viscous stress associated with the meridional flow. For the parameterization of the Reynolds stress used in our model we typically get a counterclockwise flow cell (equatorward at base and poleward at surface). This is strongly related to the radial component of the turbulent angular momentum flux, which is assumed to be directed inward in most of our models. In the absence of a meridional flow, it would increase the rotation rate at the base and decrease the rotation rate at the surface, which leads to counterclockwise Coriolis forces.

The meridional flow typically closes above $r = 0.71 R_\odot$ for two reasons. (1) The subadiabatic stratification suppresses radial motions. (2) The Reynolds stress ($\sim \nu_t$) that indirectly drives a meridional flow through a change of Ω drops significantly below $r = 0.71 R_\odot$. The meridional flow will never vanish completely in the subadiabatic region, since some radial motion is required to maintain the entropy perturbation against diffusive decay. However, the flow velocities are very small compared with the values within the convection zone. For our choice of a value of $\delta \sim -10^{-5}$, the value of v_θ is on the order of a few cm s^{-1} . For values of $\delta \sim -10^{-1}$ as found in the radiative interior, these values would drop by at least 3 orders of magnitude. The limits for the penetration of the meridional flow below the base of the convection zone are even more stringent in this model than the analysis of Gilman & Miesch (2004) showed for overshoot-like values of δ . The main reason for this is the inclusion of the feedback of the meridional flow on the differential rotation through the transport of angular momentum. Any significant equatorward flow in a region with low turbulent diffusivity would cause a retrograde zonal flow that would oppose the flow through the Coriolis force. Beside the effect of subadiabaticity to suppress radial motions, the angular momentum conservation in a low-diffusivity region yields an additional effect suppressing latitudinal motions. Only if there is a

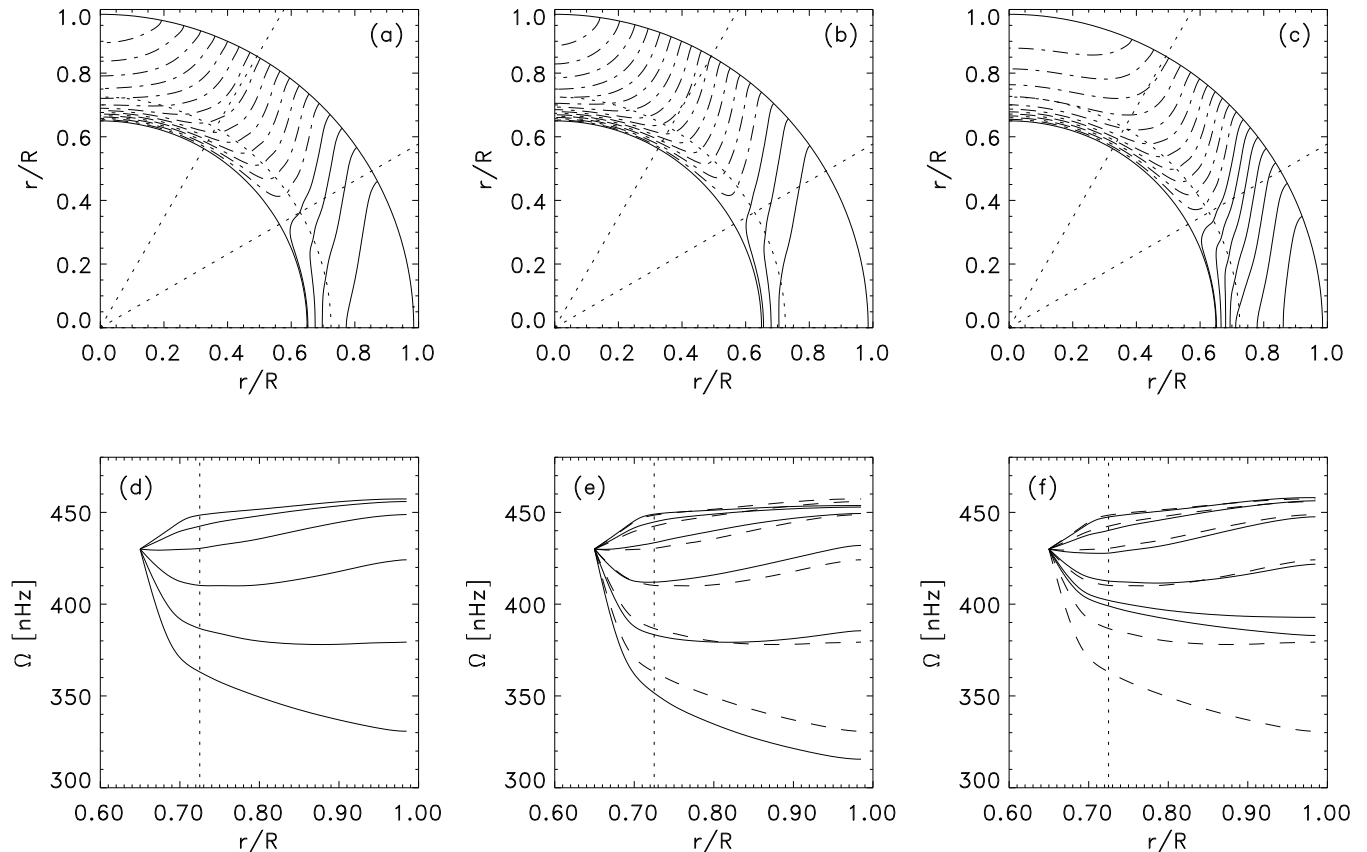


FIG. 3.— Influence of different parameterizations of the turbulent angular momentum transport on differential rotation. (a - c) Contours of the differential rotation, where solid lines indicate regions rotating faster than the core. (d - f) Profile of the differential rotation as a function of radius for the latitudes 0° , 15° , 30° , 45° , 60° , and 90° . Differential rotation is shown for (a, d) case 1 ($\lambda = 15^\circ$), (b, e) case 2 ($\lambda = 90^\circ - \theta$), and (c, f) case 4 ($\lambda = 15^\circ$ and $n = 4$). The profile of the differential rotation is rather insensitive to changes in the Reynolds stress; however, the amplitude changes, especially in high latitudes.

process that disturbs an equilibrium solution of Eq. (36) can there be a significant meridional flow below the base of the convection zone.

3.3. Dependence on parameterization of angular momentum transport

Figs. 3 and 4 show the sensitivity of the solution with respect to different parameterizations of the turbulent angular momentum transport. In cases 1 and 2 the amplitude of the angular momentum flux has the same profile in radius and latitude; however, the direction of the flow is changed. In case 1 the angular momentum is transported almost parallel to the axis of rotation with a 15° inclination angle; in case 2 the angular momentum flux has only an equatorward latitudinal component ($\lambda = 90^\circ - \theta$). In both cases the amplitude of the angular momentum flux, Λ_0 , was adjusted such that the equatorial rotation rate is the same ($\Lambda_0 = 0.8$ in case 1 and $\Lambda_0 = 0.4$ in case 2). The variation in the required amplitude follows from the fact that an angular momentum transport perpendicular to the axis of rotation is the most efficient way to speed up the rotation at the equator, whereas a transport parallel to the axis of rotation would have no effect at all. A comparison of Fig. 3, panel a) and b), shows that the profile of the differ-

ential rotation is not very sensitive to the change in the direction of the angular momentum.

Fig. 3, panels c) and f) show case 4, which is similar to case 1, but uses a turbulent angular momentum transport confined closer to the equator ($n = 4$ instead of $n = 2$). Whereas the profile of the differential rotation is only marginally changed, the magnitude of the differential rotation in high latitudes is reduced.

Unlike Ω , the meridional flow is much more sensitive to the details of the angular momentum transport. Fig. 4, panels a) to c), show the streamlines of the meridional flow, where solid lines indicate counterclockwise flows (poleward at the surface and equatorward at the base of the convection zone). Fig. 4, panels d) to f), show the latitudinal component of the meridional flow velocity at 45° latitude. All cases show a dominant counterclockwise cell; however, each case shows different flow amplitudes. The cases 1 and 3 with a significant angular momentum flux along the axis of rotation show flow velocities by a factor of around 3 larger, which is in part caused by the larger value of Λ_0 required in these cases to obtain the same equatorial rotation rate. Case 2 with angular momentum flux in latitude only also shows a weak reverse circulation cell above 60° latitude. The second cell is driven by buoyancy resulting from the higher value of

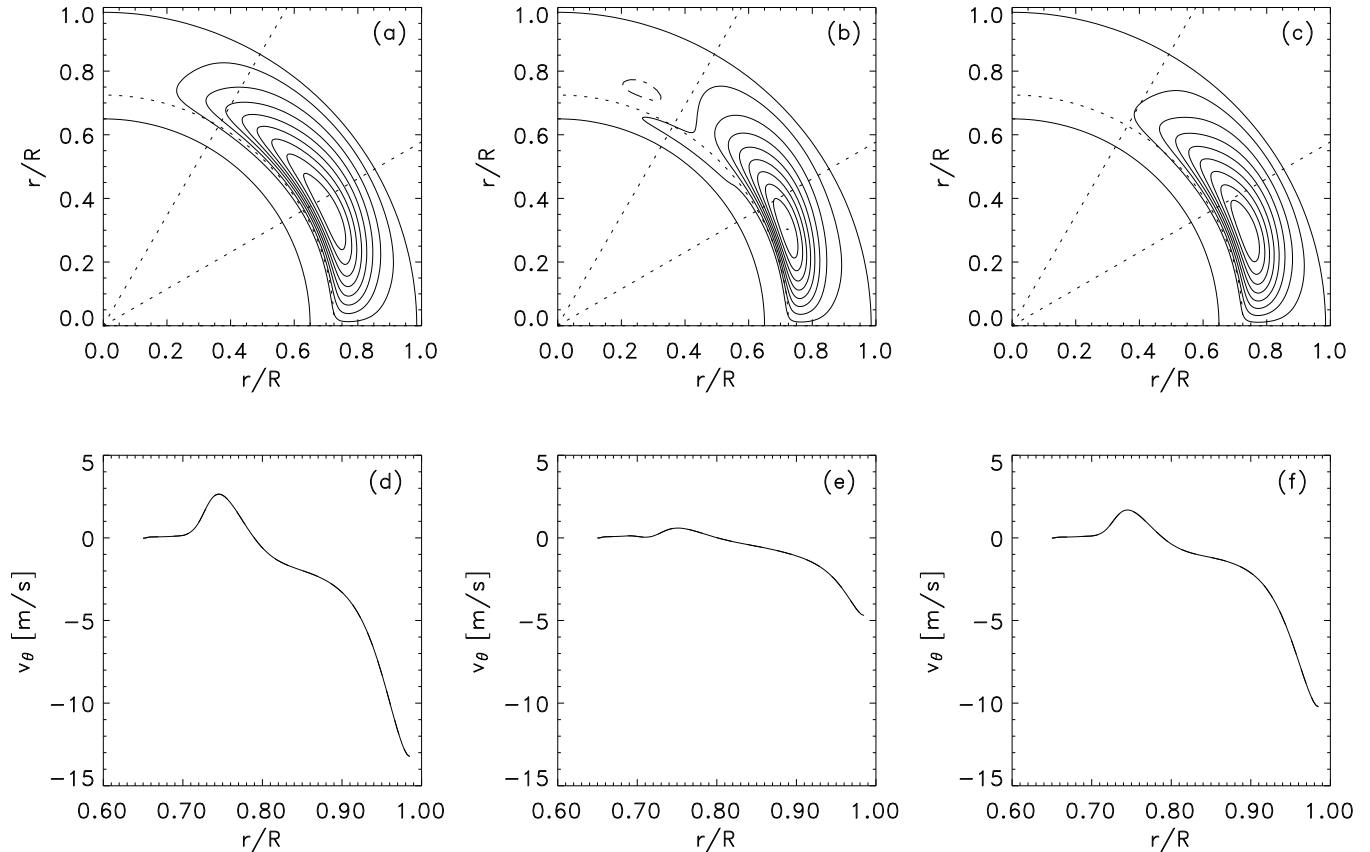


FIG. 4.— Influence of different parameterizations of the turbulent angular momentum transport on meridional flow. (a - c) Stream function, where solid lines indicate counterclockwise flows. (d - f) Radial profile of v_θ at 45° latitude. Meridional flow is shown for (a, d) case 1, (b, e) case 2, and (c, f) case 4. Unlike the differential rotation, the meridional flow is very sensitive to the direction of the angular momentum transport (compare cases 1 and 2). In case 4 the confinement of the Reynolds stress to lower latitudes also confines the meridional flow to lower latitudes.

the entropy close to the pole. This second cell is not visible in case 1, since the radial component of the angular momentum flux has a strong tendency to drive a counterclockwise meridional flow. The radially inward flux of angular momentum at high latitudes (because of the assumed 15° inclination with respect to the axis of rotation) increases the value of $\partial\Omega^2/\partial z$ in high latitudes, which leads to a counterclockwise meridional flow according to Eq. (36). There is also a very weak indication of this second cell in case 4, in which the larger value of n confines the meridional flow to lower latitudes.

The main reason for the different sensitivities of meridional flow and differential rotation with respect to changes in the Reynolds stress follows from the fact that the differential rotation is mainly determined by the balance expressed in Eq. (36). Since the entropy perturbation is not directly affected by a changing Reynolds stress, the profile of Ω also changes little. The meridional flow, on the other hand, results from an imbalance of Eq. (36) and is therefore the result of a small difference between large forces. As consequence, the sensitivity of the meridional flow to changes in the Reynolds stress is much larger.

We focus here on two distinct cases for the value of λ . We want to mention that any choice for $\lambda > 0^\circ$ and

$< 90^\circ$ leads to differential rotation close to case 1 (large values of λ are closer to the Taylor-Proudman state in low latitudes); however, the meridional flow changes significantly. Changing the value of λ requires an adjustment of $\Lambda_0 \sim 1/\sin \lambda$ in order to keep the magnitude of the differential rotation fixed. As a consequence, models with smaller values of λ have larger meridional flow velocities than models with larger values of λ . Using a value of $\lambda > 45^\circ$ also leads to a more complicated flow structure, which shows a clockwise flow pattern within most of the convection zone. Using values of $\lambda < 15^\circ$ leads to solutions very similar to case 01, but with a significantly larger amplitude of the meridional flow velocity.

3.4. Dependence on subadiabaticity, viscosity, and thermal conductivity profile

Fig. 5 compares models with identical parameterization of the Reynolds stress but different parameters for the subadiabaticity and the profiles of viscosity and heat conductivity. Panels a) and d) show how different values of the subadiabaticity affect differential rotation and meridional flow. In both panels the case 1 is shown as a reference (dashed line). Case 5 with a value of δ_{bc} twice as large shows an increase of the differential rotation by about 20%. Whereas the differential rotation remains

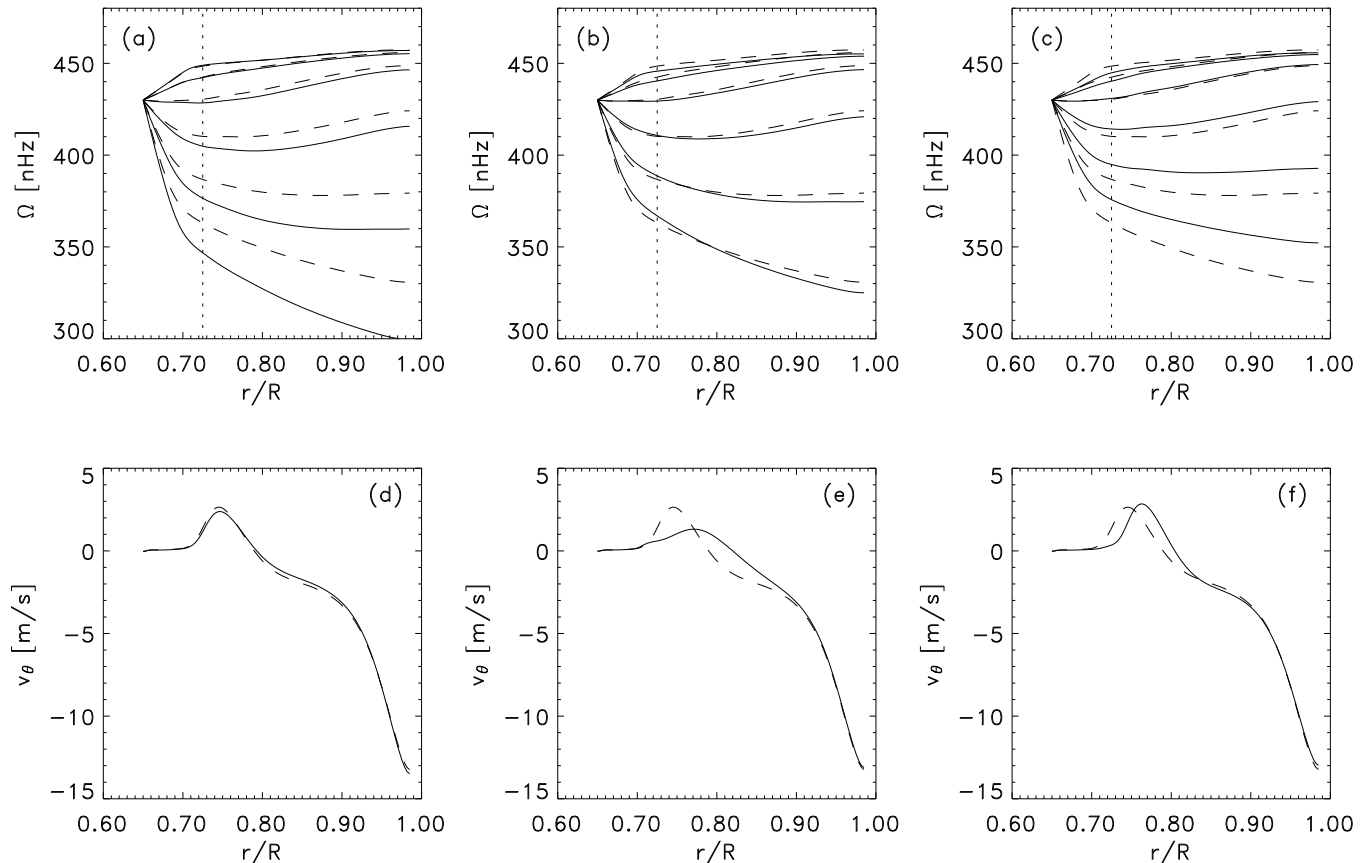


FIG. 5.— Influence of subadiabaticity, viscosity, and conductivity on solution. (a, d) Case 5 with a subadiabaticity increased by a factor of 2, leading to larger equator-pole difference in Ω but nearly no change in the meridional flow pattern. (b, e) Case 6 with an increased value of $d_{\kappa\nu}$, leading to significant reduction in the meridional flow speed. (c, f) Case 7 with a decrease in $\alpha_{\kappa\nu}$. Decreasing the overlap between the diffusivity profile and the subadiabaticity profile is very similar to decreasing the value of δ , except that the meridional return flow at the base of the convection zone is located at a different depth. In all panels we have shown case 1 as a dashed line for reference.

unchanged at the equator, the polar values of Ω decrease significantly. On the other hand, the meridional flow is only marginally affected. A larger value of δ_{bc} leads to a larger entropy perturbation, which can balance a larger differential rotation because of Eq. (36) without requiring a change of the meridional flow. A similar result can be obtained by lowering κ_0 and keeping δ_{bc} constant.

In panel b) and e) we show a solution with a factor of 2 larger width of the transition in the diffusivity profile $d_{\kappa\nu}$ (case 6). The most striking change is visible in the meridional flow pattern, where the return flow speed at the base of the convection zone is reduced by nearly a factor of 2. The amplitude of the differential rotation is only marginally affected.

Panel c) and f) shows case 7 with the parameter $\alpha_{\kappa\nu}$ decreased by a factor of 4 (value of the diffusivities at r_{tran}). The meridional flow pattern shows a reduction of the penetration into the subadiabatic layer because of the change in the Reynolds stress that drives this flow. The magnitude of the differential rotation at high latitudes decreases in response to the reduced spread of the entropy perturbation into the convection zone. Combining a lower value of $\alpha_{\kappa\nu}$ with a larger value of the subadiabaticity in the overshoot region as shown in panel (a) and c) would compensate for this effect and provide

nearly the same solution for the differential rotation (the penetration depth of the meridional flow would be still different).

So far we have discussed the influence of different profiles of viscosity and thermal diffusivity, but the magnitudes set by ν_0 and κ_0 have been left constant. We mentioned above that a change in κ_0 has the opposite effect as a change in δ_{bc} . Whereas an increase in δ_{bc} increases the entropy perturbation and through the balance Eq. (36) the differential rotation, an increase in κ_0 decreases both entropy perturbation and differential rotation. An increase in ν_0 increases the magnitude of the meridional flow and, through the term $\sim \delta v_r$ in Eq. (5), also the entropy perturbation, which also results in an increase in differential rotation. However, if ν_0 and κ_0 are changed together, the latter effect is compensated for by the larger thermal diffusivity and the differential rotation stays the same, whereas the meridional flow speed increases $\sim \nu_0$. These scalings change if ν_0 becomes so large that the viscous stress becomes a force comparable to the Coriolis force in the meridional flow equation, or if κ_0 becomes so small that advection of entropy by the meridional flow dominates over the diffusion.

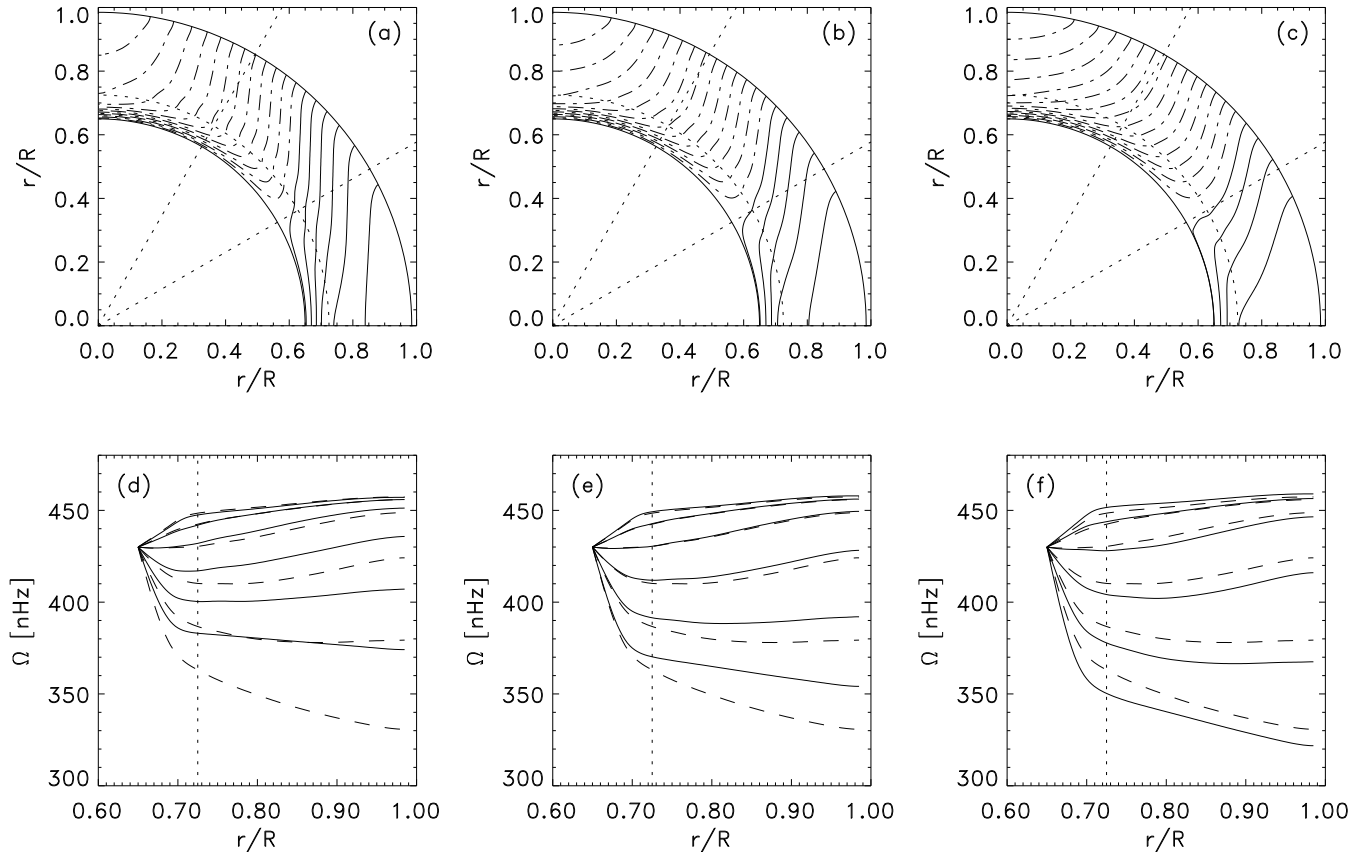


FIG. 6.— Solutions with a nonadiabatic convection zone. (a, d) Case 8 with $r_{\text{sub}} = 0.8$, (b, e) case 9 with $r_{\text{sub}} = 0.825$, and (c, f) case 10 with $r_{\text{sub}} = 0.85$. A superadiabatic convection zone can overcompensate for the effect of the subadiabatic tachocline, leading again to cylindrical differential rotation in the convection zone. However, if more than the lower third of the convection zone is weakly subadiabatic, this is sufficient to compensate for the upper superadiabatic part of the convection zone.

4. SOLUTIONS WITH NONADIABATIC CONVECTION ZONES

The models discussed so far assumed an adiabatic convection zone. This allowed us to separate the effects of a subadiabatic tachocline from processes originating within the convection zone such as the rotational anisotropy of convection, which are not considered in this model.

Since the meridional flow generates additional entropy variations in a nonadiabatic convection zone, a consideration of a more realistic stratification within the convection zone is crucial, especially since a superadiabatic stratification generates entropy variations of opposite sign. Since we are using an axisymmetric mean field approach, incorporating a superadiabatic stratification has the potential to introduce convective instability, which cannot be addressed appropriately in this model. We therefore have to make sure that with the turbulent viscosity and thermal diffusivity values we use, the Rayleigh number remains subcritical for convection. For the superadiabaticity profile defined in Eq. (25) together with a value of $\delta = 3 \times 10^{-5}$ at the top surface we have to increase the thermal diffusivity in the upper part of the convection zone to values of $5 \times 10^9 \text{ m}^2 \text{ s}^{-1}$ to avoid convective instability. We suppress here the convective

instability only by increasing κ_t , since a change of ν_t would also alter the turbulent angular momentum transport and therefore change the differential rotation and meridional flow pattern in a way that makes a comparison with the models discussed before difficult. Since we only change κ_t above r_{sub} the entropy perturbation that originates from the tachocline is only marginally affected.

Nonlocal mixing-length models as discussed by Skaley & Stix (1991) show typically below $r = 0.75$ to $0.8 R_{\odot}$ a weakly subadiabatic convection zone with values of $\delta \approx -5 \times 10^{-7}$. At $r = 0.95 R_{\odot}$ the superadiabaticity reaches values around $\delta \approx 10^{-5}$ and increases then strongly toward the surface. We cannot represent the large surface values for the reasons described above; however, as we show later, they are also not that relevant for this problem.

In Fig. 6 we shows models similar to case 1 but including a nonadiabatic convection zone as defined by Eq. (25). We have varied here the parameter r_{sub} , which determines where the convection zone turns weakly subadiabatic. In case 8 with $r_{\text{sub}} = 0.8 R_{\odot}$ (panel a) and d), the entropy perturbation arising from the superadiabatic part of the convection zone is strong enough to overpower the effect of the subadiabatic tachocline to a large extent. Below 45° latitude the differential rotation is again close to the Taylor-Proudman state with

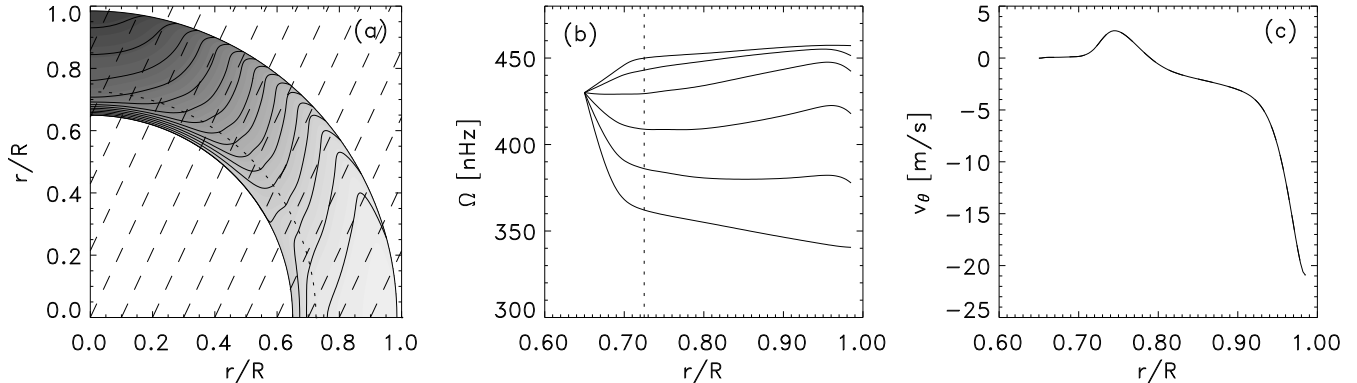


FIG. 7.— Model for values of r_{sub} between those in cases 9 and 10, with a nonvanishing inward angular momentum flux at the surface leading to a surface shear layer and an increased meridional return flow at the surface. In (a) we have overplotted dashed lines with a 25° inclination with respect to the rotation axis, which is the observed inclination of the Ω contours between 15° and 55° latitude.

cylindrical contour lines; at higher latitudes the disk like rotation contours are preserved, although the amplitude of the differential rotation is significantly reduced. Using a value of $r_{\text{sub}} = 0.85 R_\odot$ (case 10), the contribution of the subadiabatic part of the convection zone dominates over the superadiabatic top part, and a solution close to that of case 1 is retained (with slightly larger differential rotation). Comparing case 9 and case 10 shows that for the superadiabaticity profile we have chosen, the transition takes place somewhere between $r_{\text{sub}} = 0.825$ and $0.85 R_\odot$.

We found in our model that the role of a nonadiabatic convection zone depends on the extent of the weakly subadiabatic layer at the base. A transition in the solution takes place if roughly the lower 40%–50% of the convection zone is subadiabatic, even though the subadiabaticity in the lower part is very weak. Before we discuss whether such a solution is feasible at all (see next paragraph), we investigate further how sensitively this result depends on the assumption of the superadiabaticity profile within the convection zone (e.g. we did not consider the strongly superadiabatic values close to the top of the convection zone).

Eq. (20) expresses clearly that the large values of the superadiabaticity near the surface do not matter that much, since the product $\varrho_0 \delta$ is relevant. The entropy perturbation at a given latitude in the convection zone results from an efficient diffusive exchange process of the quantity $\varrho_0 T_0 s_1$ in radius, which means that the lower part of the convection zone contributes significantly, even though the value of $|\delta|$ is very small there. Consequently, if $\delta \sim \varrho_0^{-1}$, which resembles the order of magnitude variation in mixing-length models, then the contribution of the lower half of the convection zone is roughly of magnitude equal to the upper half. Therefore, if the lower half of the convection zone is weakly subadiabatic, approximately -10^{-6} to -10^{-7} , this would dominate over the contribution of the superadiabatic upper part of the convection zone.

Nonlocal mixing-length models do not provide such large subadiabatic fractions of the convection zone. Spruit (1997) suggested a highly nonlocal convection model, in which the convection is driven in a narrow su-

peradiabatic surface layer and downflows penetrate with a small amount of mixing all the way to the base of the convection zone. In this case the major fraction of the convection zone would be subadiabatic (because of radiative heating of the broad upflow in the lower convection zone), but it is unclear to what extent this model applies to solar convection.

In Fig. 7 we show a solution with a value of r_{sub} between the values used for case 9 and 10 ($r_{\text{sub}} = 0.8375 R_\odot$) and a different boundary condition for the angular velocity at the surface. Instead of setting the turbulent angular momentum transport to zero as expressed in Eq. (33), we use a radially inward transport by setting $\lambda = -\theta$ in a thin surface layer. Because of the stress-free boundary condition for Ω this requires a negative radial gradient of Ω near the surface. This parameterization reflects the idea by Gilman & Foukal (1979) that the rotational influence on supergranulation leads to an outwardly decreasing Ω .

Fig. 7 panel a) shows the differential rotation contours for this case. Over plotted are lines indicating a 25° inclination angle with respect to the axis of rotation as found by helioseismology (Schou et al. 1998, 2002). This feature is reproduced very well from about 15° to about 60° latitude. Gilman & Howe (2003) presented an explanation for this phenomenon based on the influence of a one-cell meridional flow on the differential rotation, assuming that the differential rotation would be constant in radius in the absence of the meridional flow. In our model it is difficult to identify the solution that would correspond to a solution in the absence of the meridional flow since the meridional flow is an integral part of the solution. Neglecting any effect of the meridional flow would provide a solution in which the Reynolds stress is balanced by diffusion, which in this particular case would yield contour lines with a 75° angle to the axis of rotation. In that sense the inclination is a result of the meridional flow but also including in a more complicated way the influence on the entropy profile within the convection zone.

In panel c) we show the meridional flow speed at 45° latitude. A comparison with Fig. 4 shows an increase in the surface flow speed, which is a direct result of the

changed boundary condition for the angular velocity.

We present this solution here in order to show that within the framework of this model it is possible to obtain solutions that are very close to the observed pattern by making assumptions about the superadiabaticity that go beyond the predictions of mixing-length theory (subadiabatic part of convection zone extends up to $0.8375 R_{\odot}$), but which are physically feasible if the degree of nonlocality of the convection is large enough.

5. SUMMARY

The main results of our model are as follows:

1. The profile of the differential rotation is determined mainly by the profile of the entropy perturbation originating in the subadiabatic tachocline and spreading into the convection zone because of thermal conductivity.
2. The profile of the differential rotation is rather insensitive to the parameterization of the Reynolds stress as long as there is a sufficiently large equatorward angular momentum flux; however, the magnitude of differential rotation changes with different assumptions.
3. The parameterization of the Reynolds stress strongly influences the meridional flow (compare cases 1, 2, 6, and 7).
4. If the lower half of the convection zone is weakly subadiabatic, the solar differential rotation can be explained through entropy perturbations arising from the nonadiabatic stratification. If the subadiabatic region has a smaller extent, additional effects such as anisotropic heat transport are required.
5. For angular momentum transport almost aligned with the axis of rotation and angular momentum transport in latitude only, we find a dominant counterclockwise meridional flow cell (equatorward at the base of and poleward at the upper layers of convection zone) as a robust result. Our model shows also the tendency of a weaker reverse cell at higher latitudes, which has been observed by Haber et al. (2002). A dominant counterclockwise meridional flow cell is favorable for flux-transport dynamo models, in which the equatorward meridional flow at the base of the convection zone ensures the equatorward propagation of magnetic activity through the solar cycle.
6. The meridional flow shows very little penetration beneath the base of the convection zone. In addition to the constraints imposed by the subadiabatic stratification in the radiative interior, angular momentum conservation does not allow for a significant meridional flow there, since the associated angular momentum transport would lead to significant changes of differential rotation unless opposed by a strong Reynolds stress (which is highly unlikely in the radiative interior).

6. IMPLICATION FOR SOLAR DIFFERENTIAL ROTATION

We presented in this paper a simplified model for the solar differential rotation and meridional flow. This model parametrizes important convective scale processes such as the turbulent angular momentum transport and turbulent diffusivities and does exclude processes such as rotational anisotropy of the convective energy flux as discussed in detail by Kitchatinov & Rüdiger (1995) and Küker & Stix (2001). This model is therefore not intended to be a complete differential rotation model for the solar convection zone, but rather a model to evaluate the importance of effects resulting from a nonadiabatic stratification in tachocline and convection zone.

Even though we did not use here exactly the formulation of the Λ -effect as adopted by Kitchatinov & Rüdiger (1995), Rüdiger et al. (1998), and Küker & Stix (2001) for the solar case, our results are in general agreement with their earlier work. For a magnitude of the Λ -effect (the parameter Λ_0 in our model) of order unity, we get an amplitude of the differential rotation comparable to solar values. Differences occur in the profile of the differential rotation (inclination of isolines with respect to the axis of rotation) because of the different physics considered in the entropy equation of our model (which is the main focus of this work). Larger, but explainable differences, exist in the meridional flow patterns obtained. Although the investigation of Rüdiger et al. (1998) shows a counterclockwise flow similar to our results in a model including a significant amount of viscosity and no latitudinal entropy variation, models including a latitudinal entropy gradient and a Λ -effect formulation taking into account the variation of the Coriolis number within the convection zone typically yield a clockwise flow cell close to the surface (Kitchatinov & Rüdiger 1995; Küker & Stix 2001). As explained by the authors this is because of a radially outward transport of angular momentum in the upper layers, which is not parameterized in our model. For most of our cases we assume a vanishing angular momentum flux at the surface; in the case shown in Fig. 7 we use a radially inward transport of angular momentum (as suggested by the work of Gilman & Foukal (1979) and also by observations, which clearly show a decrease of rotation rate with radius in the outer layers), which has the opposite effect of enhancing the poleward meridional surface flow. The investigation of Küker & Stix (2001) also indicates that the meridional flow is much more sensitive to details of the model used than the differential rotation (see Fig. 2 therein, which addresses the influence of the mixing-length parameter), in agreement with the findings in this paper.

The models with adiabatic convection zones, which are shown in Fig. 2 to 5, allow evaluating of the importance of the tachocline effects for models such as that of Küker & Stix (2001) that only consider the convection zone. To summarize our results, the entropy perturbation generated within a subadiabatic tachocline is strong enough to avoid the Taylor-Proudman state above 30° latitude and is therefore as important as other effects such as rotational anisotropy of the convective energy transport. However, Kitchatinov & Rüdiger (1995) found in their investigation that the effect of a subadiabatic tachocline is rather small compared with the effect of anisotropic energy transport. This apparent con-

tradition could be caused either by the different steepness of the shear profile of the differential rotation in the tachocline in the model of Kitchatinov & Rüdiger (1995) (see, e.g., Fig. 1 and 2 therein), since the magnitude of the entropy perturbation depends strongly on the value of $\partial\Omega/\partial z$, or by an insufficient overlap between thermal conductivity profile and subadiabatic overshoot region (Kitchatinov & Rüdiger (1995) computed the turbulent diffusivity through a local mixing-length relation).

Since the value of $\partial\Omega/\partial z$ within the subadiabatic tachocline is significantly larger than the value of $\partial\Omega/\partial z$ in the convection zone, the magnitude of the expected entropy perturbation in the tachocline also exceeds the magnitude required to balance a solar like differential rotation within the convection zone. If therefore only a fraction of the entropy perturbation generated within the subadiabatic tachocline spreads into the convection zone, this provides a significant contribution. This spread depends mainly on the overlap between the subadiabatic tachocline and the region that is mixed by convection. In our model we typically use a convective diffusivity of $5 \times 10^7 \text{m}^2 \text{s}^{-1}$ at $r = r_{\text{tran}} = 0.725 R_{\odot}$ and lower values below, which introduced enough coupling between the subadiabatic region and the convection zone. Since the observed tachocline spreads about one-third of the way into the region above $r = 0.713 R_{\odot}$, which is very close to adiabatic according to helioseismology (Charbonneau et al. 1999), it can be expected that there is a sufficient coupling between these two regions in the case of the Sun.

The models with a nonadiabatic convection zone (Figs. 6, 7) allow us to estimate under which conditions the entropy perturbation resulting from the nonadiabatic stratification is sufficient to explain the observed solar differential rotation without any additional effects such as anisotropic heat transport. The main problem is that a superadiabatic convection zone overcompensates the effect of the subadiabatic tachocline to a large degree unless the lower half of the convection zone is weakly subadiabatic. Even though the absolute values of the superadiabaticity in the convection zone are much lower than those in the tachocline, their contribution can be very large because of the much larger radial meridional flow velocity within the convection zone. We found that the effect of the superadiabatic part of the convection zone can be compensated by a weakly subadiabatic lower half of the convection zone, since the thermal inertia of the entropy perturbation is $\sim \varrho_0 T_0 s_1$ and therefore even a small entropy perturbation at the base of the convection zone can contribute more than a large entropy perturbation in the upper part of the convection zone. Within the frame work of this model we cannot address the question of whether such a solution is feasible, since this would require more sophisticated nonlocal convection theory. Nonlocal mixing-length models typically predict a subadiabatic stratification below $r = 0.8 R_{\odot}$; however, for a larger degree of nonlocality (stable downflows with only little entrainment and detrainment) a larger extent of this region would be possible. If additional effects such

as anisotropic heat transport and nonlinear feedback of the stratification on the heat conductivity were included, it could be possible that a solar-like solution as shown in Fig. 7 is possible with a smaller extent of the subadiabatic part of the convection zone.

A further test of the process proposed in this paper would be the inclusion of a subadiabatic tachocline in the full spherical shell convection simulations. Besides adding a subadiabatic overshoot region, this requires the inclusion of the tachocline shear layer either by resolving the relevant physical processes or by forcing the shear (as done in this model) through a lower boundary condition, since the entropy perturbation arises as a consequence of a subadiabatic shear layer. Since the entropy perturbation is also affected significantly by the meridional flow within a nonadiabatic convection zone, it is also crucial to get the meridional flow pattern right. Work in this direction is currently in progress.

Since the meridional flow is of high interest for flux transport dynamos, here we discuss in more detail the findings of our model concerning the penetration of the return flow below the base of the convection zone. As mentioned above, our model provides a counterclockwise flow as a robust result, provided that there is an inwardly directed turbulent angular momentum flux. The return flow at the base of the convection zone is located in the region with the largest turbulent viscosity gradient, since there the divergence of the turbulent angular momentum flux (Λ -effect) would lead to an increase of rotation rate unless opposed by an equatorward transport of angular momentum by the meridional flow (which tends to slow down the rotation rate). In that way the meridional flow is always tied to the presence of turbulent Reynolds stress. For the parameterization of the turbulent diffusivities we use in most of our models, the meridional flow speed at $r = 0.71 R_{\odot}$ typically drops to less than 10% of the maximum return flow speed, which is reached at around $r = 0.745 R_{\odot}$. Below $r = 0.71 R_{\odot}$ velocities on the order of a few cm s^{-1} persist, however our model tends to overestimate their amplitude since we use overshoot values for δ . Using radiative core values would decrease this amplitude further by several orders of magnitude. Therefore, a penetration of the meridional flow below the base of the convection zone as used in a few flux transport dynamo models seems very unreasonable, since it implies that there are very strong Reynolds stresses in the strongly subadiabatic radiative core. Since the constraint set by the angular momentum conservation is additional to the constraint set by the subadiabaticity of the stratification, which was pointed out by Gilman & Miesch (2004), the limitation on penetration of meridional flow beneath the base of the convection zone is even more stringent than found by Gilman & Miesch (2004).

The author wants to thank P. A. Gilman and M. S. Miesch for stimulating discussions about the solar differential rotation problem.

REFERENCES

- Braun, D. C. & Fan, Y. 1998, *ApJ*, 508, L105
 Brun, A. S. & Toomre, J. 2002, *ApJ*, 570, 865
 Charbonneau, P., Christensen-Dalsgaard, J., Henning, R., Larsen, R. M., Schou, J., Thompson, M. J., & Tomczyk, S. 1999, *ApJ*, 527, 445

- Durney, B. R. 1999, *ApJ*, 511, 945
—, 2003, *Sol. Phys.*, 217, 1
- Gilman, P. A. & Foukal, P. V. 1979, *ApJ*, 229, 1179
- Gilman, P. A. & Howe, R. 2003, in *ESA SP-517: GONG 2002. Local and Global Helioseismology: the Present and Future*, 283
- Gilman, P. A. & Miesch, M. S. 2004, *ApJ*, 611, 568
- Gilman, P. A. & Miller, J. 1986, *ApJS*, 61, 585
- Glatzmaier, G. A. & Gilman, P. A. 1982, *ApJ*, 256, 316
- Haber, D. A., Hindman, B. W., Toomre, J., Bogart, R. S., Larsen, R. M., & Hill, F. 2002, *ApJ*, 570, 855
- Küker, M. & Stix, M. 2001, *A&A*, 366, 668
- Kitchatinov, L. L., Pipin, V. V., & Ruediger, G. 1994, *Astronomische Nachrichten*, 315, 157
- Kitchatinov, L. L. & Rüdiger, G. 1993, *A&A*, 276, 96
—, 1995, *A&A*, 299, 446
- Labonte, B. J. & Howard, R. 1982, *Sol. Phys.*, 80, 361
- Miesch, M. S., Elliott, J. R., Toomre, J., Clune, T. L., Glatzmaier, G. A., & Gilman, P. A. 2000, *ApJ*, 532, 593
- Pidatella, R. M. & Stix, M. 1986, *A&A*, 157, 338
- Rempel, M. 2004, *ApJ*, 607, 1046
- Rüdiger, G., von Rekowski, B., Donahue, R. A., & Baliunas, S. L. 1998, *ApJ*, 494, 691
- Schou, J., Antia, H. M., Basu, S., Bogart, R. S., Bush, R. I., Chitre, S. M., Christensen-Dalsgaard, J., di Mauro, M. P., Dziembowski, W. A., Eff-Darwich, A., Gough, D. O., Haber, D. A., Hoeksema, J. T., Howe, R., Korzennik, S. G., Kosovichev, A. G., Larsen, R. M., Pijpers, F. P., Scherrer, P. H., Sekii, T., Tarbell, T. D., Title, A. M., Thompson, M. J., & Toomre, J. 1998, *ApJ*, 505, 390
- Schou, J., Howe, R., Basu, S., Christensen-Dalsgaard, J., Corbard, T., Hill, F., Komm, R., Larsen, R. M., Rabello-Soares, M. C., & Thompson, M. J. 2002, *ApJ*, 567, 1234
- Skaley, D. & Stix, M. 1991, *A&A*, 241, 227
- Spruit, H. 1997, *Memorie della Societa Astronomica Italiana*, 68, 397
- Stix, M. 1981, *A&A*, 93, 339
- Topka, K., Moore, R., Labonte, B. J., & Howard, R. 1982, *Sol. Phys.*, 79, 231
- Zhao, J. & Kosovichev, A. G. 2004, *ApJ*, 603, 776